Available online at www.sciencedirect.com
SCIENCE DIRECT®
Journal of volcanology and geothermal research
ELSEVIER
Journal of Volcanology and Geothermal Research 131 (2004) 165–178
www.elsevier.com/locate/jvolgeores

The impact of side wall cooling on the thermal history of lava lakes

Lars H. Rüpke *, Matthias Hort

GEOMAR Research Center, Department of Volcanology and Petrology, Wischhofstr. 1-3, 24148 Kiel, Germany

Received 10 September 2002; accepted 26 September 2003

Abstract

Most simple models for cooling of sheet like intrusions, the Hawaiian lava lakes being one example, neglect the effect of side wall heat loss on the overall thermal evolution. In this paper we extend a conventional one-dimensional (1D) model for cooling of sheet like intrusions to account for lateral heat loss by either prescribing a fixed side wall heat flux, or a heat flux controlled by heat transport in the surrounding wall rock. In the first part of the study we analyze the general interplay between side wall cooling and the thermal evolution of the system; the second part focuses on a comparison between our modeling results including models without and with lateral heat flux, and the Hawaiian lava lake data. This comparison leads to the following three main conclusions: (1) Side wall cooling does have a significant impact on the cooling history of lava lakes. (2) Models assuming a time dependent temperature profile in the wall rock lead to a better fit with the measured temperature data. (3) Due to the sluggish conductive heat transfer in the mush its thermal evolution is significantly decoupled from the temperature evolution of the convecting bulk liquid.

Keywords: lava lakes; modeling; magma chambers; lateral cooling

1. Introduction

Cooling and crystallization processes are the keys to understanding the evolution of oceanic and continental crust. How exactly cooling and crystallization interact during the solidification of magma is a vigorous matter of research (e.g. Bergantz, 1995; Jaupart and Tait, 1995; Hort, 1997; Jellinek and Kerr, 2001) and over the past decades crystallization inside magmatic intrusions has been studied with several different numerical models (e.g. Peck et al., 1977; Peck, 1978; Worster et al., 1990, 1993; Hort, 1997). Most of these models assume sheet like geometries, so that lateral heat loss is negligible in the cooling process, save for the models by Oldenburg and Spera (1992) (see also Spera et al., 1995). For this reason, the interaction of lateral heat loss and the thermal evolution of moderately non-sheet like magmatic bodies remains somewhat unexplored. One would expect that for aspect ratios (height to width) smaller than 0.05 (typical for dikes and sills, Marsh, 2000) side wall cooling becomes negligible, but in the case of aspect ratios between

* Corresponding author.
E-mail address: lruepke@geomar.de (L.H. Rüpke).

0377-0273/03/$ – see front matter © 2003 Elsevier B.V. All rights reserved.
doi:10.1016/S0377-0273(03)00361-5

Table 1
Complete list of symbols and parameters used in the model formulation

Parameter	Description	Value	Units
C	constant in Rayleigh–Nusselt relationship	–	–
C'	constant in crystal growth function	–	–
F_b	convective heat flux from bulk liquid through solidification front	–	–
F_{wr}	lateral and basal heat flux	–	–
H	height of the system	–	m
K	Boltzmann constant	1.38×10^{-23}	J K^{-1}
L	latent heat	3.35×10^{5}	J kg^{-1} K^{-1}
Nu	Nusselt number	–	–
R	radius	–	m
Ra	Rayleigh number	–	–
T	temperature	–	K
T_L	liquidus temperature	1473	K
T_S	solidus temperature	1243	K
T_t	surface temperature	–	K
T_i	interface temperature	–	K
T_b	bulk liquid temperature	–	K
T_{wr}	wall rock temperature	–	K
T_m	temperature in the mush	–	K
T_o	initial temperature in Eqs. 1 and 2	–	K
U_{max}	amplitude of the growth rate function	–	–
U^*	normalized growth rate function	–	–
$U(T)$	parameterized growth rate function	–	–
a	width	–	m
b	depth	–	m
c	specific heat	1100	J kg^{-1} K^{-1}
g	gravitational acceleration	9.81	m s^{-2}
h_i	position of the solidification front	–	m
h'_i	normalized position of the solidification front	–	–
k	thermal conductivity	–	W m^{-1} K^{-1}
r	radial distance	–	m
r^*	normalized radial distance	–	–
t	time	–	s
x	horizontal coordinate	–	m
x^*	normalized horizontal coordinate	–	–
y	horizontal coordinate	–	m
y^*	normalized horizontal coordinate	–	–
z	vertical coordinate	–	m
z^*	normalized vertical coordinate	–	–
α	thermal expansion constant	10^{-4}	K^{-1}
κ	thermal diffusivity	6×10^{-6}	m^2 s^{-1}
$\gamma = a/H = b/H = R/H$	aspect ratio	–	–
$\tau = t\kappa/H^2$	dimensionless time	–	–
θ_x	normalized temperature	–	–
ϕ_x	crystallinity	–	–
λ	empirical constant in Eq. 9	0.056	–
μ	viscosity	–	Pa s
μ_L	viscosity at the liquidus temperature	50	Pa s
ρ	density	2600	kg m^{-3}
ΔG_{ae}^{ba}, ΔG_{ae}^{ab}	activation energies	–	–
$T_{wr_{init}}$	initial wall rock temperature	600	K
∇T_{wr}	prescribed temp. gradient in the wall rock	140	K m^{-1}

The subscript x either stands for mush m, interface i, or bulk liquid b.

0.1 and 0.4, typical for the Hawaiian lava lakes, cooling through the sides should be of some importance and should therefore be taken into account when developing models for the cooling and crystallization of such intrusions.

In order to test down to what aspect ratios side wall cooling is of importance a simple comparison between models for the cooling of an infinite sheet (one-dimensional, 1D), the cooling of an infinite rod (two-dimensional, 2D) and of a box (three-dimensional, 3D) can be made based on simple analytical and numerical solutions of conductive cooling. Cooling of an infinite sheet with a constant initial temperature T_o and boundaries held at zero temperature is given by (Carslaw and Jaeger, 1959, p. 97, eq. (8)):

$$T(z,t) = \frac{4T_o}{\pi}\sum_{n=0}^{\infty}\frac{(-1)^n}{2n+1}\exp\left(-\frac{(2n+1)^2\pi^2 t\kappa}{4H^2}\right)\cos\left(\frac{(2n+1)\pi z}{2H}\right). \quad (1)$$

Here H is the thickness of the sheet, κ is the thermal diffusivity, and t is time in seconds. A complete list of symbols is given in Table 1. Here the origin of the coordinate system is centered in the middle of the sheet. Integrating Eq. 1 over the thickness of the entire sheet and over time yields the average temperature inside the sheet as a function of time (Carslaw and Jaeger, 1959, p. 97, eq. (10)):

$$T_{av}\frac{8T_o}{\pi}\sum_{n=0}^{\infty}\frac{1}{(2n+1)^2}\exp\left(-\frac{(2n+1)^2\pi^2\kappa t}{4H^2}\right). \quad (2)$$

With the boundary conditions specified above even analytical solutions for the evolution of temperature for the 2D case:

$$T(y,z,t) = T(y,t)T(z,t) \quad (3)$$

and the 3D case:

$$T(x,y,z,t) = T(x,t)T(z,t)T(y,t) \quad (4)$$

exist (see Carslaw and Jaeger, 1959, p. 173, eq. (11) for the 2D case and p. 34, eq. (10) for the 3D case). Introducing the height to width ratio $\gamma = a/H$ with a being the width of the 2D box and $\gamma = a/H = b/H$ with a being the width and b being the depth of the 3D box along the x,y-axes, and defining $y = z\gamma$ (2D case) and $x = y = z\gamma$ (3D case) Eqs. 3 and 4 may be rewritten such that:

$$T(\gamma,z,t) = T(\gamma z,t)T(z,t) \text{ and } T(\gamma,z,t) = T^2(\gamma z,t)T(z,t). \quad (5)$$

In principle Eq. 5 can be integrated analytically just like Eq. 1 to come up with a value for T_{av} for the 2D and 3D cases but the expressions become very lengthy after a while and therefore Eq. 5 was integrated numerically to calculate the average temperatures. While varying the height to width ratio, the volume of the 3D model was kept constant to ensure comparability between the different runs.

Fig. 1 shows the average temperature inside the different geometries as a function of the height to width ratio, γ. Of course, in the 1D case, this ratio does not make sense, here it refers to the normalized thickness of the sheet. Clearly the differences in temperatures decrease when γ decreases and for $\gamma < 0.1$ there is no significant difference any more. However, for $\gamma = 0.4$ the normalized average temperatures vary between 0.63 (1D), 0.54 (2D) and 0.46 (3d), which is a significant (27%) decrease. Even for $\gamma = 0.2$ the difference is still larger than 20% (0.41, 0.37, 0.32) and at $\gamma = 0.1$ it is 17%.

This simple estimate demonstrates that side wall cooling in not too 'sheet like' systems does play an important role and has to be accounted

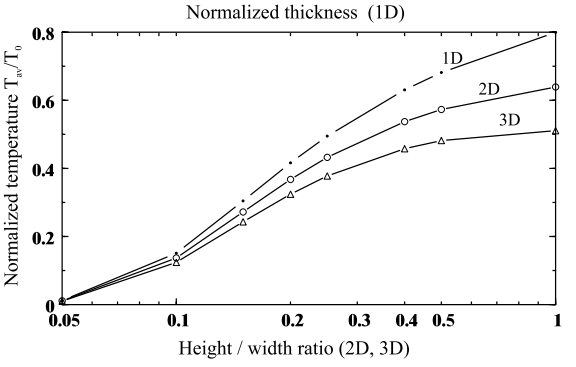

Fig. 1. Comparison of the temperatures inside an infinite sheet (dots), an infinite rod (circles) and a box (triangles) as a function of the height to width ratio γ. In the case of $\gamma = 1$ the thickness $2H$ was equal to 20 m and shown is the average temperature inside the different bodies after 36 days.

for. However, the impact of convection on the whole cooling still needs to be explored in such systems, and in the following part of the paper we present a numerical model for the cooling of sheet like bodies including lateral heat loss. This allows us to analyze lateral cooling and its impact on the crystallization history of magmatic intrusions. We do this by assuming different geometries, varying wall rock temperatures, and constant versus time dependent lateral heat fluxes. To cross-check our model, we compare the results to data collected at the Hawaiian lava lakes Makaopuhi, Kilauea Iki, and Alae. This comparison shows that the predicted temperatures and crust locations fit the measured data well, which shows that our modeling approach is a valid approximation to the processes inside lava lakes. In addition, we find that although lava lakes usually have aspect ratios < 0.2, side wall cooling does indeed have a significant influence on their cooling history.

2. The model

A variety of different modeling approaches exist for the cooling and crystallization behavior of fluids with the simplest case being a one-component fluid that is cooled from above. This problem was first solved by Stefan (1891) and has subsequently been called the Stefan problem. It reduces to two possible states within the system: The fluid's temperature can be above the liquidus temperature and no crystals exist or the fluid completely solidifies upon the temperature dropping below the liquidus temperature. One of the major assumptions made in the Stefan problem is that the phase transition takes place at a fixed temperature, the liquidus temperature, implying that crystallization is an equilibrium process. In this case the advance rate of the solidification front is exclusively controlled by the amount of latent heat release during solidification.

For top-down crystallizing multicomponent melts like magma, the situation is more complicated. The different components typically solidify over a temperature range of $\sim$200°C, so that crystallization is a continuous process that starts at the liquidus temperature and is complete at the solidus temperature. The solidification of magma is associated with strong changes in physical properties with the dramatic viscosity increase – by a factor of 10^{16} – likely to be the most important. Magma viscosity plays an important role in the stratification and thereby cooling of a magmatic intrusion. It has been found that maximum packing of solids for basaltic magmas occurs at a crystallinity of about 55% consistent with the results of drilling experiments at the now solidified historic Hawaiian lava lakes. To drill through the solid upper portion of a lava lake, the drilling stem had to be mechanically advanced until the lava's crystallinity dropped below 55% at which point the drilling stem sank under its own weight (Wright and Okamura, 1977; Helz, 1980). Although the exact viscosity at this point is unknown, this observation suggests that this point marks the transition from mainly solid like to mainly fluid like behavior. Below this upper crust a mushy region exists; a mush is a region characterized by the coexistence of a stationary crystal matrix and interstitial melts. Note that this definition of a mushy region would of course also include the upper partially crystallized rigid crust. However, due to the change in mechanical properties at the point of 55% crystallization we use this criterion for the distinction between the rigid crust and the mushy region. A volume occupied by a multicomponent melt that is cooled from above will therefore separate in different parts (Fig. 2) that following Marsh (1989a) can be called (a) upper crust (here the degree of crystallization is between 50 and 100%), (b) a mushy region (here the temperature is at or lower than the liquidus temperature and the melt is only crystallized up to 50%), and (c) an underlying bulk liquid where the temperature is still higher or equal to the liquidus temperature and no crystals exist. The boundary between the mushy layer and the bulk liquid is called the solidification front and in this case marks the appearance of the first crystals.

The major problem in extending the one-component Stefan-type solution to such a magmatic multicomponent system is hidden in the equilibrium assumption that is applied at the solidification front. If a magma is not superheated, which is a

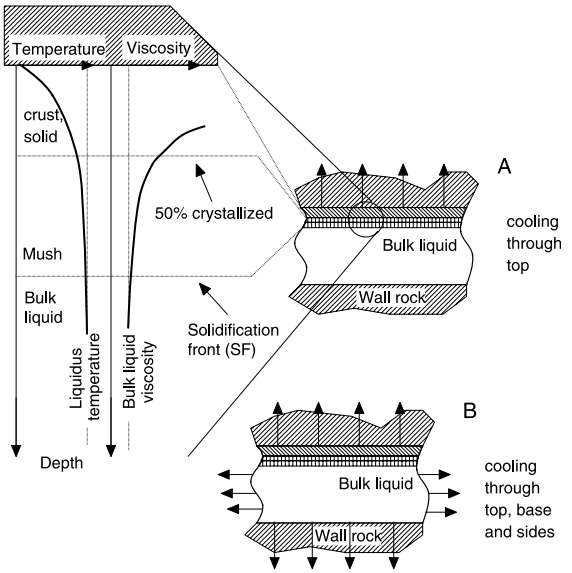

Fig. 2. Schematic drawing of the model geometry showing the general features of the mushy model as well as the whole system once being only cooled from the top (A) and once through the top, base, and sides (B).

common situation (e.g. Turner et al., 1986; Marsh, 1996), the equilibrium model breaks down and the speed of the solidification front becomes infinite (Worster et al., 1990), because no latent heat needs to be released in order to advance the solidification front. One way to cope with this problem is to use a disequilibrium model which requires a certain amount of undercooling below the liquidus temperature to initiate the phase transition. In this case the speed of the solidification front is equal to the crystal growth rate which is controlled by the degree of undercooling (e.g. Kerr et al., 1990b). With the undercooling necessary for crystal growth, there is also a temperature difference between the solidification front and the bulk liquid that may drive convective motion in the whole system. This temperature difference is a minimum estimate for the temperature difference available to drive thermal convection, as part of the overlying mush may or may not go unstable too (see e.g. Davaille and Jaupart, 1993; Marsh, 1989b). In case of convection the solidification front now separates the convecting bulk liquid and the non-convecting mush; it no longer marks the appearance of the first crystals in the liquid as the temperature in the bulk liquid may drop below the liquidus temperature leading to internal crystallization (e.g. Hort, 1997; Jellinek and Kerr, 2001).

None of the models proposed so far for the cooling and crystallization of lava lakes did include the cooling through the sides; cooling through the top has been investigated several times and cooling through top and bottom once (Worster and Huppert, 1993). In this paper we construct a rather simple model for accounting for lateral heat loss by assuming a cylindrical geometry instead of a sheet like geometry. In order to calculate the loss of heat through either top, bottom or the sides, we split the problem into two 1D problems, meaning we once determine the heat flux through top and bottom using the standard extended Stefan model solution, and once through the mantle of the cylinder either by prescribing a heat flux or calculating the heat flux into the surrounding country rock. The loss of heat through all sides is then used to calculate the change in bulk liquid temperature.

We readily admit that using this approach we slightly underestimate the total loss of heat from the system. This can easily be shown through the analytical model discussed above. From Eq. 1 we can calculate the flux of heat through one side. Multiplying this flux by 6 (the cube has six sides) and integrating it over time we can calculate the average temperature inside the cube if heat is lost through each side 'one-dimensionally'. The error by which we overestimate the average temperature compared to the full 3D conductive solution (Eq. 4) is on the order of 10%. We therefore believe that our approach is a good first order approximation to the problem and certainly a lower limit estimate, so it is conservative. The model constructed in the following section extends the ideas of the 1D model presented earlier by Kerr et al. (1990b), Worster et al. (1993) and Hort (1997)).

2.1. Temperature in the mush

We assume that heat transport in the solid and mushy part of the system is exclusively conductive. Neglecting convection in these parts is of course a simplification especially if the mush is

porous. However, Hort (1997) argued that this assumption does not alter the cooling process significantly. We therefore describe the temperature distribution in the mush by the 1D heat conduction equation:

$$\rho c\frac{\partial}{\partial t}T_{\mathrm{m}} = k\frac{\partial^2}{\partial z^2}T_{\mathrm{m}} + \rho L\frac{\partial}{\partial t}\phi_{\mathrm{m}}. \quad (6)$$

Here z, t, ρ, c, k, L, T, ϕ are the vertical coordinate, time, density, specific heat, thermal conductivity, latent heat, temperature, and degree of crystallization, respectively. In order to simplify the nomenclature of our variables we also introduced an index notation, where the subscript m refers to variables in the mush, subscript i refers to the solidification front, subscript b describes the bulk liquid, and finally the parameters of the surrounding wall rock are labeled with the index wr. We calculate the degree of crystallization by assuming a linear relationship between the temperature and crystallinity:

$$\phi_x = \frac{T_{\mathrm{L}} - T}{T_{\mathrm{L}} - T_{\mathrm{S}}} \quad (7)$$

which is a valid first order approximation to the true phase relations (Hort, 1997). The subscript x in Eq. 7 either stands for mush (m) or bulk liquid (b), and subscripts L, S for liquidus and solidus, respectively. In this formulation of the crystallinity–temperature relation we implicitly assume that there is no bulk compositional stratification during the solidification process, so that the solidus and liquidus temperature in Eq. 7 are independent of time and position.

2.2. Bulk liquid temperature and lateral heat loss

Conservation of heat provides the basis for calculating the temperature evolution of the bulk liquid. The heat flux out of the bulk liquid has to be balanced by the loss of sensible heat from the bulk liquid diminished by the latent heat released due to internal crystallization in the bulk liquid. Here we assume equilibrium crystallization in the bulk liquid which has been shown to be a very good approximation to this part of the system (Hort, 1997). We decompose the net heat flux out of the bulk liquid into the convective heat flux F_{b} through the top and the lateral and basal heat flux F_{wr} and express the thermal evolution of the bulk liquid as:

$$\rho(H-h_{\mathrm{i}})\left(c\frac{\partial}{\partial t}T_{\mathrm{b}} - L\frac{\partial}{\partial t}\phi_{\mathrm{b}}\right) = -F_{\mathrm{b}} - F_{\mathrm{wr}}. \quad (8)$$

This formulation implies that the bulk liquid in the interior of the solidifying magma is always well mixed, so that its temperature remains uniform. This approximation is justified, since we assume that the bulk liquid is constantly convecting throughout the model runs thereby suppressing any thermal or chemical stratification. We further assume that internally grown crystals participate in the convective motion and do not sediment to the ground. This is of course a simplification since basal heat loss may potentially lead to some thermal stratification at the base of the system as well as sedimenting crystals may form a basal boundary layer. Such a boundary layer may result in a slightly diminished heat loss through the base of the system that is not accounted for in our model formulation.

The convective heat flux out of the bulk liquid through the mush, F_{b}, is determined from the well known Rayleigh–Nusselt relationship which expresses the Nusselt number as a function of the Rayleigh number (see e.g. Kerr et al., 1990a), so that $Nu = CRa^b$. In this formulation C is a constant and b typically varies between 1/3 and 1/4 (Marsh, 1989b). In this study we assume $b = 1/3$, which is typical for convection driven by cooling from top and heating from below. The value of the Nusselt number itself is defined as the ratio of the actual heat flux, F_{b}, compared with purely conductive heat flux F_{CD}, so that $Nu = F_{\mathrm{b}}/F_{\mathrm{CD}}$. Using the definition of the Rayleigh number $Ra = (g\rho\alpha(T_{\mathrm{l}} - T_{\mathrm{i}})H^3)/(\kappa\mu)$ and applying Fouriers law, $q = k\nabla T$, with k being the thermal conductivity, for the conductive heat flux, F_{CD}, we express the convective heat flux as (e.g. Turner, 1979):

$$F_{\mathrm{b}} = 2^{\frac{4}{3}}\lambda k\left(\frac{\alpha g\rho}{\kappa\mu_{\mathrm{b}}}\right)^{\frac{1}{3}}(T_{\mathrm{b}} - T_{\mathrm{i}})^{\frac{4}{3}}. \quad (9)$$

Here λ is an empirical constant, μ the viscosity, α the thermal expansion coefficient, k the thermal diffusivity and $(T_{\mathrm{b}} - T_{\mathrm{i}})$ the difference between

the bulk liquid temperature, T_b, and the interface temperature, T_i. We use a value of 0.056 for λ as suggested by Kerr et al. (1990a). We hasten to emphasize that the above formulation of the Rayleigh number describes systems that are heated from below or cooled from above, but not systems that are additionally cooled from the sides. Since side wall cooling is an additional source of negative buoyancy, the used Rayleigh number can only be regarded as a lower bound for the true Rayleigh number, but in order to allow a direct comparison to the models with no side wall cooling we use this standard definition of the Rayleigh number.

Close examination of Eqs. 6 and 8 shows that lateral heat transport exists exclusively from the bulk liquid into the surrounding wall rock. Neglecting the conductive heat flux from the mush into the wall rock is justified by the fact that lateral heat transfer in it is not nearly as efficient as in the bulk liquid. Furthermore, as explained above, we assume that the directions of the basal and lateral heat flows are strictly vertical and horizontal.

To calculate the heat flux through the sides and the bottom of the system, F_{wr}, we assume a cylindrical geometry. In this scenario F_{wr} can be calculated from:

$$F_{wr} = k_{wr}\left(\frac{\partial}{\partial z}T_{wr}\bigg|_{z=H} + \frac{\partial}{\partial r}T_{wr}\bigg|_{r=R} 2\gamma(1-h'_i)\right) \quad (10)$$

where the first term in the brackets is the flux through the base of the system and the second term the flux through the sides. In Eq. 10 r is the horizontal radial distance from the center of the bulk liquid, h'_i is the normalized location of the solidification front ($h'_i = h_i/H$), and γ is the aspect ratio of the intrusion (H/R). In our experiments we use two different approaches to calculate the two heat flux terms on the right-hand side of Eq. 10: We either set them to a fixed value or solve for the time dependent temperature distribution inside the wall rock. In this latter case we solve the heat conduction equation in cartesian coordinates for the heat loss through the bottom and in cylindrical coordinates for the lateral heat loss.

2.3. Temperature at the interface

The last piece missing in the model formulation is the boundary condition at the moving solidification front. Conservation of heat requires that latent and sensible heat and the convective heat flux from the bulk liquid across the solidification front have to be balanced by the conductive heat flux into the mush:

$$\rho c(T_b - T_i)\frac{\partial}{\partial t}h_i + \rho L(\phi_i - \phi_b)\frac{\partial}{\partial t}h_i + F_b = k\frac{\partial}{\partial z}T_m\bigg|_{z=h_i}. \quad (11)$$

Here h_i is the location of the solidification front, ϕ_i and ϕ_b are the degrees of crystallization at the solidification front and in the bulk liquid, T_m describes the temperature in the mush and T_i the one at the interface. The first term on the left-hand side describes the amount of sensible heat while the second term is the latent heat released.

In the classical one-component Stefan problem, the interface temperature, T_i, equals the liquidus temperature and the degree of crystallization at the interface jumps from 0 to 100%. In this case the speed of the solidification can be determined directly from Eq. 11. In a multicomponent system with disequilibrium crystallization, a certain amount of undercooling is necessary for crystals to grow and the interface temperature is no longer equal to the liquidus temperature. Consequently, the fraction crystallized at the interface, ϕ_i, being a function of T_i, is now greater than zero and does not jump to 100% any more. To cope with this problem, we set the speed of the solidification front, $\partial h_i/\partial t$, equal to the rate of crystal growth – as calculated from the crystal growth function (see Spohn et al., 1988; Worster et al., 1990; Hort, 1997).

Crystal growth is a thermally activated process and can be written as the difference between the activation energy needed to integrate a molecule into the crystalline structure, ΔG_{ae}^{ba}, and the one needed to disintegrate it, ΔG_{ae}^{ab} (Rao and Rao, 1978):

$$U = C'\left\{\exp\left(-\frac{\Delta G_{ae}^{ba}}{KT}\right) - \exp\left(-\frac{\Delta G_{ae}^{ab}}{KT}\right)\right\} \quad (12)$$

where K is the Boltzmann constant and C' a con-

Table 2
Values used for the dimensionless numbers in the standard model formulation

Parameter	Description	Value
S	Stefan number	1.3
θ_t	dimensionless surface temperature	−4
Γ	growth rate constant	500
T_u*	norm. temperature maximizing $U(T)$	0.95
γ	aspect ratio	0.1
Ra_0	initial Rayleigh number	10^{14}

stant. In this formulation, the crystal growth function still contains the different activation energies which are mostly unknown and therefore make modeling difficult. However, following Spohn et al. (1988), Eq. 12 may be parameterized by using the fact that the crystal growth function has a maximum at the temperature T_u. We can now rewrite the crystal growth function in a more convenient way:

$$U(T) = U_{max}\frac{(T_L - T)T_u}{(T_L - T_u)T}\exp\left(\frac{T_L(T-T_u)}{T(T_L-T_u)}\right) = U_{max}U^*(T). \quad (13)$$

For the temperature T_u and the maximum amplitude $U(T_u) = U_{max}$ we use literature values as they are tabulated in e.g. Dowty (1980) and set the rate of crystal growth equal to speed of the solidification front in Eq. 11:

$$\frac{\partial}{\partial t}h_i = U(T) = U_{max}U^*(T). \quad (14)$$

Before solving the system of equations we nondimensionalized the governing equations by introducing the dimensionless temperature $\theta = (T - T_S)/(T_L - T_S)$ and the dimensionless time scale $\tau = (t\kappa)/(H^2)$, where H is the height of the system and $\kappa = k/(\rho c_p)$ the thermal diffusivity. For the full dimensionless model formulation and the numerical details please refer to Appendix A and Table 2.

3. Modeling results

We analyze the impact of lateral heat loss on the thermal evolution of the system by comparing the results of a reference model which is exclusively cooled from above with the results of models that are additionally cooled from the base or from the sides and the base.

3.1. The reference model

Fig. 3 shows a typical thermal evolution of magma cooled from above; the locations of the solidification front and the crust–mush boundary (here the degree of crystallization reaches 50%) are plotted in Fig. 3a as solid and dashed lines, respectively. The origin of the parabolic shape (typical to the classical Stefan solution) can be understood if one analyzes what happens if the solidification front advances by a small amount: Upon advancement a certain amount of heat is transferred from the bulk liquid and the solidification front through the mush to the surface. This heat consists of three parts, the latent and sensible heat released (a) in the mush, (b) at the advancing solidification front, and (c) in the bulk liquid. The first part (a) is controlled by the temperature pro-

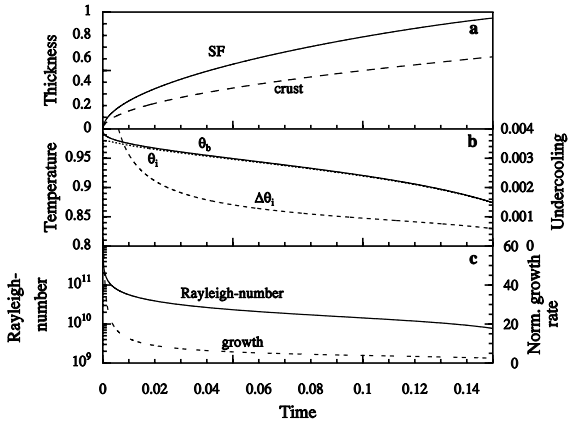

Fig. 3. A typical thermal history of magma that is exclusively cooled from above. See the text for a detailed explanation. SF = solidification front.

file in the mush, while the other two parts (b and c) are functions of the interface temperature, θ_i, and the bulk liquid temperature, θ_b (all temperatures are normalized temperatures, see Appendix A). Since conservation of heat is required at the solidification front, the total amount of heat transferred from the bulk liquid and the solidification front has to be equal to the amount of heat that can be transferred to the surface by conduction through the mush. This value is controlled by the heat flux through the mush that decreases when the mush thickens thus decreasing the amount of heat that can be conducted through it. Therefore the heat flux inside the mush is the factor limiting the rate of advancement of the solidification front and the crust giving rise to the nearly parabolic shape of the curves.

At time zero the interface temperature equals the surface temperature and consequently the undercooling at the interface, $\Delta\theta_i = \theta_l - \theta_i$, driving the advancement of the solidification front, is high. Here θ_l is the current liquidus temperature and because we assume equilibrium crystallization in the bulk liquid it equals θ_b. Because the crystal growth rate is a strong function of the undercooling, the large undercooling results in a high rate of advancement of the solidification front that explains the initially rapid growth shown by the solid line in Fig. 3a.

Since we assume equilibrium crystallization in the bulk liquid, no bulk liquid undercooling exists at any time. The degree of crystallization of the bulk liquid follows directly from Eq. 7. The temperature difference, $\Delta\theta_c = \theta_b - \theta_i$, that drives convection is equal to the undercooling, $\Delta\theta_i = \theta_l - \theta_i$, at the interface driving the growth of crystals and thereby advance of the solidification front. Therefore, during the early stages of cooling not only the crystal growth rate is high as a result of the high undercooling (see Fig. 3c), $\Delta\theta_i$, but also convective cooling of the bulk liquid is strong (see Fig. 3c). Thus the bulk liquid temperature θ_b drops and internal crystallization occurs. This is accompanied by latent heat release.

As stated before, the latent and sensible heat released in the bulk liquid at the interface and in the mush have to be transferred to the surface. Since conduction eventually becomes too sluggish to transfer these initially significant amounts of heat to the surface due to thickening of the mush, the amount of undercooling (see Fig. 3b), $\Delta\theta_i$, has to decrease reducing the advance of the solidification front (see Fig. 3a) and the cooling of the bulk liquid (Fig. 3b) and therefore the latent heat production. Note, since we use a linear relationship between temperature and crystallinity (Eq. 7) in all figures the degree of internal crystallization can always be directly determined from the bulk liquid temperature ($\phi_b = (1-\theta_b)$).

Fig. 3b shows that a certain undercooling, $\Delta\theta_i$, equal to the driving force of convection, $\Delta\theta_c$, is present throughout the entire solidification. The resultant convective heat flux F_b out of the bulk liquid lowers the bulk liquid temperature θ_b continuously (Fig. 3b). If, however, the bulk liquid temperature dropped below the interface temperature θ_i convection would cease and the bulk liquid temperature would remain constant. This case was, however, never observed during the model calculations and convection is thus always present. It may occur, when one models the crystallization in the bulk liquid as a disequilibrium process (see Hort, 1997).

3.2. The impact of heat loss through the sides

To explore how extra lateral and basal cooling may affect the solidification process we compare the reference model (solid lines) to models that are additional cooled by a time dependent basal (dashed lines) and basal plus lateral (dotted lines) heat flux (Fig. 4). As one would expect the additional cooling leads to a faster drop in the bulk liquid (θ_b) and interface temperature (θ_i) (see Fig. 4b,c). However, when looking at the positions of the solidification front and the crust (Fig. 4a) a somewhat counter intuitive behavior is observed. The speed of the crust–mush boundary increases, while the advancement of the solidification front slows down.

To understand the influence of extra side wall cooling on the location of the crust–mush boundary the definitions of the solidification front and the crust–mush boundary are important. We defined the crust–mush boundary as the boundary where 50% of the melt is crystallized whereas the

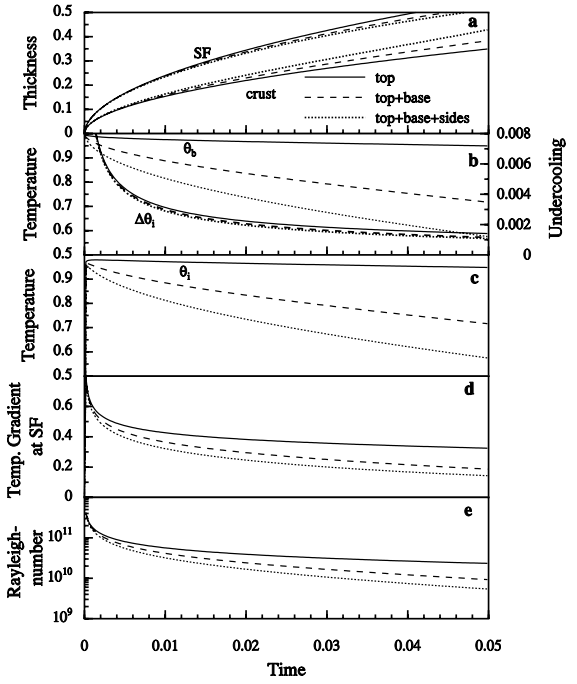

Fig. 4. Comparison of the thermal evolution of magma being cooled from above (solid lines), from the top and the base (dotted lines), and from the top, the base and the sides assuming $\gamma = 0.5$ (dashed lines). Heat transport in the country rock is assumed to be by heat conduction, so the heat flux term in Eq. 11 is directly evaluated from the appropriate heat conduction equation. SF = solidification front.

solidification front separates the convecting from the non-convecting part of the system. The degree of crystallization at the crust–mush boundary is therefore always constant, while the fraction crystallized at the interface does not have a fixed value, it depends on the interface temperature θ_i and this value varies significantly between models.

Since the degree of crystallization is directly linked to the temperature (see Eq. 7), lateral and basal cooling change the temperature and crystallinity profile within the mush thereby modulating the speed of the crust–mush boundary that increases with additional cooling. The average temperature inside the mush is lower if the system is cooled from the sides which increases the degree of crystallization. At every point in time the point where 50% crystallinity is reached is therefore deeper inside the system compared to the case of insulated sides; consequently the rate of advancement of the crust–mush boundary is higher.

The explanation for the slower solidification front is somewhat more complicated. As a direct consequence of the extra cooling the bulk liquid temperature, θ_b and the temperature at the solidification front, θ_i, drop more rapidly (Fig. 4b,c) meaning the degree of crystallization at the solidification front is not the same in the different model calculations shown in Fig. 4. This makes the comparison between the solidification front positions in the different model calculations difficult and allows only a qualitative discussion. As the degree of crystallization in the bulk liquid increases with additional cooling, the amount of latent heat that is produced in the bulk liquid also increases with additional cooling. From Eq. 11 it is clear that the conductive heat flux into the mush must equal the amount of latent and sensible heat released at the solidification front plus the convective heat flux F_b. Because the heat flux into the mush diminishes faster if the system is cooled from all sides (Fig. 4d) than in the case of exclusive cooling from the top, the amount of heat that can be transported to the surface decreases faster. If the amount of latent and sensible heat from the bulk liquid increases and if the heat flux into the mush decreases, the amount of latent heat that can be removed from the solidification

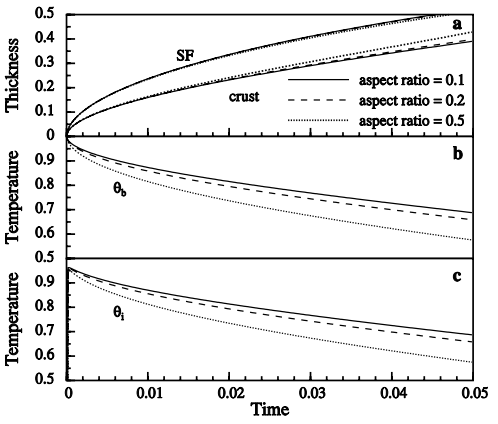

Fig. 5. The impact of differing aspect ratios γ on the thermal evolution of the system. The solid lines refer to a model that assumes an aspect ratio of 0.1, the dashed lines to one with $\gamma = 0.2$, and the dotted lines to one with $\gamma = 0.5$. SF = solidification front.

front decreases and therefore its speed reduces as is observed in the model calculations.

One aspect of side wall cooling – which we do not explicitly explore in the model calculations – is that mushy layers may also develop along the sides and the base of the system. One potential effect of these fronts is that the aspect ratio, γ, of the system continuously changes. Fig. 5 shows the evolution of the solidification front, the upper crust position, and the bulk liquid temperature for models that account for lateral cooling, but assume different aspect ratios between 0.1 and 0.5. The impact of varying γ on the location of the crust and solidification front is negligible; the bulk liquid and interface temperature decrease slightly with an increasing aspect ratio as one would expect. One effect not included in the model calculation might be that the temperature gradient at the margins of the bulk liquid might be smaller if mushy layers were allowed to develop along them. Therefore, the lateral heat losses assumed in this study represent the maximum cooling rate for a given geometry and initial wall rock temperature.

Next we will fit measured temperature data in the historic Hawaiian lava lakes by adjusting the amount of lateral and basal heat loss. Here, the actual values given for these extra heat fluxes can be viewed as effective heat fluxes through the potentially 'mushy' sides and base of the lakes.

4. Applying the model on lava lake cooling

The three historic Hawaiian lava lakes Alae, Makaopuhi, and Kilauea Iki have been subject to extensive field work including temperature measurements and estimates of the upper crust locations (Wright and Okamura, 1977; Peck, 1978), which allows us to benchmark our modeling results against these data sets. Fig. 6 shows a comparison between the measured and modeled crust locations (Fig. 6, upper part) and bulk liquid temperatures (Fig. 6, lower part) for different kinds of model calculations. These are the reference model and models additionally cooled from the base and sides by a constant or time dependent heat flux. The vertical error bars in Fig. 6,

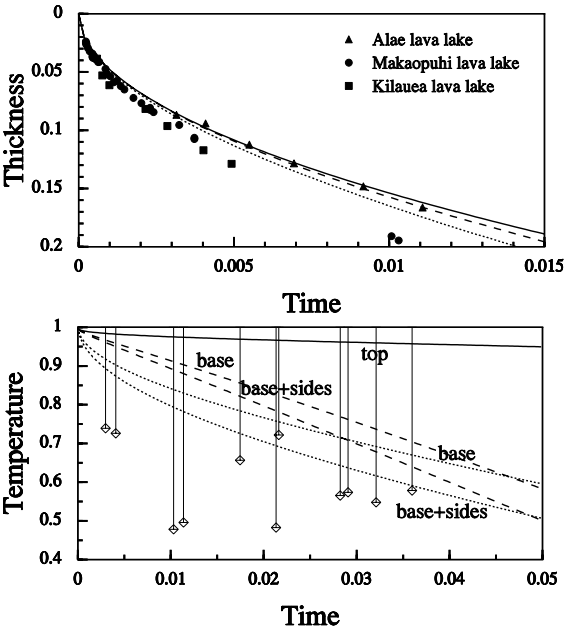

Fig. 6. Comparison of various model calculations to data collected in the Hawaiian lava lakes. In the models with a constant heat flux through the bottom and the sides a value of 70 W/m^2 has been assumed which was found to give a good fit to the data at later times. For a description on how the error bars on the measured temperature data are generated the reader is referred to the text.

lower part stem from the impossibility to drill through the mush all the way into the bulk liquid and directly measure the bulk liquid temperature. The measured temperatures can therefore only give a lower bound to the true bulk liquid temperature which can be anywhere between the measured value and the initial liquidus temperature.

To better compare the measured data with our modeling results we non-dimensionalize all values. To do so, we need the thickness of the lava lakes as well as the thermal diffusivity, κ, of the melts that filled the lava lakes. We use the depths of the three different lava lakes as given in the various drilling reports (13.7 m (Alae), 83 m (Makaopuhi), 111 m (Kilauea Iki)) and use the generally accepted value of 6.0×10^{-7} m^2/s for κ.

Fig. 6, upper part shows that all different models fit the measured crust locations quite well with the models including extra cooling from the sides and/or the base leading to a better fit of the data. Also the measured bulk liquid temperatures,

shown in Fig. 6, lower part, are much better fitted by models including extra cooling than by the reference model. In this case, however, there is a remarkable difference between the different types of models: A constant heat flux generally leads to an overestimate of the bulk liquid temperature early on during the cooling history while a time dependent heat flux results in a better fit to the measured data. In addition, there is a significant offset between models that are additionally cooled from below and models that lose heat to all sides although we have assumed the typically small value of 0.2 for the aspect ratio in the calculations.

5. Discussion and conclusions

The incorporation of side wall heat loss into a standard 1D model for cooling of sheet like geometries led to three main conclusions. First, the model calculations demonstrate the significance of side wall cooling for the crystallization history of lava lakes. The offset in the modeling results between models that are cooled from the top and bottom and models that also include side wall cooling shows that despite the small aspect ratio ($\gamma = 0.2$) lateral heat loss does have a significant impact on the thermal evolution of sheet like intrusion in general and lava lakes in particular. Second, the fact that models assuming a constant heat flux in the wall rock seem to overestimate the bulk liquid temperature during early times of the cooling which suggests that side wall heat flux is indeed a function of time. Third, we have shown that additional heat loss through the sides and base of the system does not have a strong influence on the location of the upper crust. This behavior indicates that there is a decoupling between the parts of the system that are cooled by conduction and those cooled by convection. The temperature distribution in the mush appears therefore to be shielded from the processes inside the bulk liquid.

Acknowledgements

We would like to thank Ross Kerr and Bruce Marsh for a helpful and thorough review of this paper. Many thanks also to Chantal Tisseau, René Maury, and Thierry Juteau for their help while L.H.R. was at the IUEM and the Université de Bretagne Occidentale. Support from the graduate school 'Dynamics of Global Cycles' at Kiel University is also greatly appreciated.

Appendix A. Numerics

Here we derive the full set of dimensionless equations used in the model derived above. We non-dimensionalize the governing equations by scaling length with H, time with H^2/κ, where κ is the thermal diffusivity $\kappa = k/\rho c$, and temperature with $\Delta T = T_L - T_S$ and then introducing θ as the dimensionless temperature $\theta = (T - T_S)/\Delta T$. Using those scales we derive the following set of dimensionless variables:

τ is the dimensionless time:

$$\tau = \frac{t\kappa}{H^2},$$

z^* and r^* are the new distance coordinates:

$$z^* = \frac{z}{H},\ r^* = \frac{r}{R},$$

and h'_i is the normalized location of the solidification front:

$$h'_i = \frac{h_i}{H}.$$

Introducing these variables into the governing equations provides the new set of dimensionless equations. Eq. 6, describing the temperature distribution in the mush, now takes the following form:

$$\left(1 - \frac{\partial}{\partial \tau}\phi_m S\right)\frac{\partial}{\partial \tau}\theta_m = \frac{\partial^2}{\partial z^{*2}}\theta_m. \tag{A.1}$$

The temperature at the solidification front, earlier described by Eq. 11, is expressed as:

$$((\theta_b - \theta_i) + S(\phi_i - \phi_b))\frac{\partial}{\partial \tau}h'_i + Nu^*\left(\frac{1}{\mu'}\right)^{\frac{1}{3}}(\theta_b - \theta_i)^{\frac{4}{3}} = \frac{\partial}{\partial z^*}\theta_m\Big|_{z^* = h'_i}, \tag{A.2}$$

the bulk liquid temperature (Eq. 8) as:

$$(1-h'_i)\left(\frac{\mathrm{d}}{\mathrm{d}\tau}\theta_b - S\frac{\mathrm{d}}{\mathrm{d}\tau}\phi_b\right) = -Nu^*\left(\frac{1}{\mu'}\right)\frac{1}{3}(\theta_b-\theta_i)\frac{4}{3} - \frac{\partial}{\partial z^*}\theta_{wr}\Big|_{z^*=1} + 2\gamma(1-h'_i)\frac{\partial}{\partial r^*}\theta_{wr}\Big|_{r^*=1}. \quad (A.3)$$

Finally the temperature distribution in the wall rock is rewritten as:

$$\frac{\partial}{\partial\tau}\theta_{wr} = k\frac{\partial^2}{\partial r^{*2}}\theta_{wr}. \quad (A.4)$$

The term μ' in Eq. A.2 is the dimensionless viscosity:

$$\mu' = \frac{\mu}{\mu_L}, \quad (A.5)$$

with μ being the viscosity and μ_L the viscosity at the liquidus temperature. Following Hort (1997), Eq. A.5 may be rewritten such that:

$$\mu' = \exp\left(\frac{T_u^*}{1-T_u^*}\frac{1-\theta_b}{\theta_b+B}\right). \quad (A.6)$$

Here $B = T_S/\Delta T$ is a constant, θ_b is the dimensionless bulk liquid temperature and $T_u{}^* = T_u/T_L$.

The parameters appearing in the dimensionless Eqs. A.1–A.4 are a Stefan number S:

$$S = \frac{L}{c\Delta T}, \quad (A.7)$$

a modified Nusselt number Nu^*:

$$Nu^* = 2\frac{4}{3}\lambda\left(\frac{Ra_0}{1-\theta_t}\right)\frac{1}{3}, \quad (A.8)$$

and the initial Rayleigh number Ra_0:

$$Ra_0 = \frac{\alpha g\rho(T_L-T_t)H^3}{\kappa\mu_L}. \quad (A.9)$$

Finally the crystal growth function (Eq. 14) has to be scaled as well. This is done by introducing the growth law constant $\Gamma = U_{max}H/\kappa$:

$$\frac{\mathrm{d}}{\mathrm{d}\tau}h'_i = \Gamma U^*. \quad (A.10)$$

Following Kerr et al. (1990a) the moving boundary problem is solved by mapping the interval $[0\ldots h'_i]$ linearly on the interval $[0\ldots1]$.

To actually solve the governing differential equations numerically, some initial and boundary conditions have to be set. The initial conditions are:

$$\begin{aligned}&\theta_b(\tau=0)=1,\\ &\phi_b(\tau=0)=0,\\ &h'_i(\tau=0)=0,\end{aligned} \quad (A.11)$$

while the boundary conditions are:

$$\begin{aligned}&\theta_m(z^*=0,\tau)=\theta_t,\\ &\theta_m(z^*=h'_i,\tau)=\theta_i,\\ &\theta_{wr}(r^*=0,\tau)=\theta_b,\\ &\theta_{wr}(r^*\to\infty,\tau)=\theta_{wr_{init}}.\end{aligned} \quad (A.12)$$

The initial condition for θ_b implies that the erupted lava is not superheated which is true for most lavas (see above). Even if it is superheated it has been shown that convective processes in lava cooled from above rapidly remove any existing superheat (Turner et al., 1986). The boundary condition for the wall rock temperature θ_{wr} is found by assuming that the temperature far away from the contact (here a distance of $5H$ is assumed) is not altered by the heat flux from the lava lake and stays therefore constant. It is also assumed that the surface temperature θ_t remains constant as a result of air circulation.

After all initial and boundary conditions are set, the differential equations are solved using finite differences. Since all equations are coupled they cannot be solved independently from each other. Eq. A.10, describing the rate of advancement of the solidification front, is substituted into Eq. A.2 and solved together with the heat conduction equation for the temperature in the mush Eq. A.1. This is done by varying the dimensionless interface temperature θ_i and solving the differential equations accordingly until Eq. A.2 is satisfied to a prescribed accuracy. The implemented algorithm uses an iterative Crank–Nicholson technique to solve the partial differential Eq. A.1 while the search for θ_i in Eq. A.2 is done by using a combined root bracketing, bisection, and inverse quadratic interpolation method also

known as Brent's method (Press et al., 1992). To determine the temperature in the bulk liquid, θ_b, the ordinary differential Eq. A.3 is integrated together with the partial differential Eq. A.4. For the ordinary differential equation a fourth order Runge–Kutta algorithm is utilized while the partial differential equation is solved with the already mentioned Crank–Nicholson technique.

References

Bergantz, G.W., 1995. Changing techniques and paradigms for the evaluation of magmatic processes. J. Geophys. Res. 100, 17603–17613.

Carslaw, H.S., Jaeger, J.C., 1959. Conduction of Heat in Solids. Clarendon, Oxford.

Davaille, A., Jaupart, C., 1993. Thermal convection in lava lakes. Geophys. Res. Lett. 20, 1827–1830.

Dowty, E., 1980. Crystal growth and nucleation theory and numerical simulation of igneous crystallization. In: Hargraves, R.B. (Ed.), Physics of Magmatic Processes. Princeton University Press, Princeton, NJ, pp. 419–486.

Helz, R.T., 1980. Crystallization history of Kilauea Iki lava lake as seen in drill cores recovered in 1967–1979. Bull. Volcanol. 43, 675–701.

Hort, M., 1997. Cooling and crystallization in sheet-like magma bodies revisited. J. Volcanol. Geotherm. Res. 76, 297–317.

Jaupart, C., Tait, S., 1995. Dynamics of differentiation in magma reservoirs. J. Geophys. Res. 100, 17615–17636.

Jellinek, A.M., Kerr, R.C., 2001. Magma dynamics, crystallization, and chemical differentiation of the 1959 Kilauea Iki lava lake, Hawaii, revisited. J. Volcanol. Geotherm. Res. 110, 235–263.

Kerr, R.C., Woods, A.W., Worster, M.G., Huppert, H.E., 1990a. Solidification of an alloy cooled from above Part 1. Equilibrium growth. J. Fluid Mech. 216, 323–342.

Kerr, R.C., Woods, A.W., Worster, M.G., Huppert, H.E., 1990b. Solidification of an alloy cooled from above Part 2. Non-equilibrium interfacial kinetics. J. Fluid Mech. 217, 331–348.

Marsh, B.D., 1989a. Magma chambers. Annu. Rev. Earth Planet. Sci. 17, 439–474.

Marsh, B.D., 1989b. On convective style and vigor in sheet-like magma chambers. J. Petrol. 30, 479–530.

Marsh, B.D., 1996. Solidification fronts and magmatic evolution. Min. Mag. 60, 5–40.

Marsh, B.D., 2000. Magma chambers. In: Sigurdson, H. (Ed.), Encyclopedia of Volcanoes. Academic Press, San Diego, CA, pp. 191–206.

Oldenburg, C.M., Spera, F.J., 1992. Modeling transport processes in nonlinear systems: The example of solidification and convection. In: Yuen, D.A. (Ed.), Chaotic Processes in Geological Sciences. Springer, New York, pp. 205–224.

Peck, D.L., 1978. Cooling and vesiculation of Alae lava lake, Hawaii. US Geol. Surv. Prof. Pap. 935, 1–60.

Peck, D.L., Hamilton, M.S., Shaw, H.R., 1977. Numerical analysis of lava lake cooling models: Part II, Application to Alae lava lake, Hawaii. Am. J. Sci. 277, 415–437.

Press, W.H., Teukolsky, S.A., Vetterling, W.T., Flannery, B.P., 1992. Numerical Recipes. Cambridge University Press, Cambridge.

Rao, C.N.R., Rao, K.J., 1978. Phase Transition in Solids. McGraw Hill, New York.

Spera, F.J., Oldenburg, C.M., Christensen, C., Todesco, M., 1995. Simulations of convection with crystallization in the system $KAlSi_2O_6$–$CaMgSi_2O_6$: Implications for compositionally zoned magma bodies. Am. Mineral. 80, 1188–1207.

Spohn, T., Hort, M., Fischer, H., 1988. Numerical simulation of the crystallization of multicomponent melts in thin dikes or sills 1. The liquidus phase. J. Geophys. Res. 93, 4880–4894.

Stefan, J., 1891. Über die Theorie der Eisbildung, insbesondere über die Eisbildung im Polarmeere. Ann. Phys. Chem. 98, 269–286.

Turner, J.S., 1979. Buoyancy Effects in Fluids. Cambridge University Press, Cambridge.

Turner, J.S., Huppert, H.E., Sparks, R.S., 1986. Komatiites II: Experimental and theoretical investigation of post-emplacement cooling and crystallization. J. Petrol. 27, 397–437.

Worster, M.G., Huppert, H.E., 1993. The crystallization of lava lakes. J. Geophys. Res. 98, 15891–15901.

Worster, M.G., Huppert, H.E., Sparks, R.S.J., 1990. Convection and crystallization in magma cooled from above. Earth Planet. Sci. Lett. 101, 78–89.

Worster, M.G., Huppert, H.E., Sparks, R.S.J., 1993. The crystallization of lava lakes. J. Geophys. Res. 98, 15891–15901.

Wright, T.L., Okamura, R.T., 1977. Cooling and crystallization of tholeiitic Basalt, 1965 Makaopuhi lava lake, Hawaii. US Geol. Surv. Prof. Pap. 1004, 1–78.